Numerical Integration of the Blade-to-Blade Surface Euler Equations in Vibrating Cascades

G. A. Gerolymos*
SNECMA, Moissy Cramayel, France

The unsteady aerodynamics of fluttering cascades is a demanding problem in the analysis of modern compressors. An algorithm has been developed for numerically integrating the Euler equations in blade-to-blade surface formulation. The method simulates all the interblade channels of an annular cascade. The equations are discretized in a grid that moves in order to follow the vibration of the blades. The equations are integrated using the explicit MacCormack scheme in finite-difference formulation. Mistuned vibration as well as standing-, traveling-, or influence-wave modes may be readily simulated. Also, two other faster methods have been developed, simulating traveling and influence waves, respectively. A number of numerical results show the aptitude of the method to simulate both started and unstarted supersonic flow in vibrating cascades. A first comparison with available wind-tunnel data corroborates the validity of this approach to predict supersonic flutter of fans and compressors.

Nomenclature

a = speed of sound
b = streamsheet thickness
${}^1C_p$ = pressure coefficient first harmonic $\{{}^1C_p = {}^1p/(p_{t_{rel}} - p)_{inlet}\ \delta_{vib}]\}$
f = vibration frequency
F = flux vector, Eq. (2)
h = enthalpy
H = vector of nonconservative quantities, Eq. (2)
I = rothalpy $[I = h + W^2/2 + (\Omega R)^2/2]$
IW = influence-wave method
m = meridian coordinate
M = Mach number
M_{is} = isentropic Mach number $\{M_{is} = \sqrt{2/\gamma - 1[(p_{tinlet}/p)^{\gamma - 1/\gamma} - 1]}\}$
MC = multichannel method
N = number of blades
Ni, Nj = number of grid points in I and J, respectively
p = pressure
q = dissipation coefficient, Table 1
q = generalized displacements vector, Eq. (5)
r = traveling-wave order
R = radius
R_g = gas constant
Sr_χ = Strouhal number based on chord length $[Sr_\chi = (f \cdot \chi/W_{inlet})]$
t = time
T = temperature
TW = traveling-wave method
U = vector of unknowns, Eq. (2)
W = relative velocity
(X, Y) = computational plane Cartesian coordinates system, Eq. (4)
β_r = interblade phase angle, Eq. (5)
δ_{vib} = vibratory amplitude $[\delta_{vib} = \max_k(\max_{\text{blade surface}} \sqrt{\delta_x^2 + \delta_y^2})/\chi]$
ϑ = angular coordinate
ρ = density
χ = chord length
ω = vibration angular frequency
Ω = rotational angular velocity
ϕ = nodal diameters

Subscripts
i,j = grid indices
t = stagnation conditions
k = number of blade
rel = relative frame
m = meridianwise
ϑ = pitchwise
X = Xwise
Y = Ywise

Superscripts
$\overline{\ }$ = mean value between leading and trailing edge, Eq. (4)
α, β = indices equal to 0 or 1, Table 1
n = time level, Table 1
p = projected values, Table 1
$*$ = predictor values
$**$ = corrector values, Table 1
1 = first harmonic, Table 1
T = transpose of a vector

Introduction

FLUTTER inception may limit compressor operation at various regions of the compressor operating map (Fig. 1).[1] That is why flutter analysis has become part of the design process of aircraft engine axial compressors.[2] To this end, unsteady aerodynamics codes have been developed. Early work in the field concentrated on simplified semi-analytical methods.[3-5] Their major drawback was that they had to make restrictive assumptions on cascade geometry. However, the availability of modern high-speed computers[6-9] enhanced the development of more accurate numerical methods. Both potential methods[10-13] and Euler solvers[14,15] have appeared in the literature.

In this work, we are primarily interested in supersonic flutter (regions 2, 3, and 4 in Fig. 1). The relative upstream Mach number at the blade tip sections is supersonic, and the

Received March 16, 1987; revision received April 13, 1988.

*Research Engineer, Aerodynamics Department, Villaroche Research Center.

flow may be started or unstarted, depending on back-pressure level.[16,17] Experimental results[18,19] and theoretical analyses[20,21] have stressed the importance of shock-wave oscillation in supersonic flutter and have suggested that the shock-wave motion may be nonharmonic even when the structural vibration is harmonic. On the other hand, viscous effects do not seem dominant in the region of supersonic flutter. That is why the Euler equations seem to be well adapted to the problem.

We have developed a method for analyzing the unsteady aerodynamics of vibrating compressor cascades. The flow is modeled by the unsteady Euler equations, written on a streamsheet generated by revolution of a meridian streamline, following Wu's quasi-three-dimensional model (Fig. 2).[22] The time dependence of the streamsheet radial position and thickness constitute unsteady three-dimensional effects. They are omitted in the context of quasi-three-dimensional theory.[4] Then the unsteady blade-to-blade surface Euler equations are

$$\frac{\partial U}{\partial t} + \frac{\partial}{\partial m} F_m(U) + \frac{\partial}{R\,\partial \vartheta} F_\vartheta(U) + H(U) = 0 \tag{1}$$

with

$$U = (\rho bR,\quad \rho b\,RW_m,\quad \rho bRW_\vartheta,\quad \rho bRI - bRp)^T \tag{2a}$$

$$F_m = (\rho bRW_m,\quad \rho bRW_m^2 + bRp,\quad \rho bRW_mW_\vartheta,\quad \rho bRW_mI)^T \tag{2b}$$

$$F_\vartheta = (\rho bRW_\vartheta,\quad \rho bRW_\vartheta W_m,\quad \rho bRW_\vartheta^2 + bRp,\quad \rho bRW_\vartheta I)^T \tag{2c}$$

$$H = \left(0,\quad -p\frac{\partial bR}{\partial m} - \rho b\,(W_\vartheta + \Omega R)^2 \frac{\partial R}{\partial m},\quad \rho b\,W_m(W_\vartheta + 2\Omega R)\frac{\partial R}{\partial m},\quad 0\right)^T \tag{2d}$$

and are completed by the perfect-gas equation of state

$$p = \rho R_g T \tag{3}$$

The integration of these equations with steady-state boundary conditions converges asymptotically to the steady-state solution.[23] Their integration in a vibrating cascade determines the response of the flowfield to the oscillations of the blades.

Computational Mesh

Initial Grid

The blade-to-blade surface is mapped into the computational plane by the transformation[24]

$$(X,Y)^T = (m,\bar{R}\vartheta)^T \tag{4}$$

which unfolds the blade-to-blade surface in both the circumferential and the meridian direction. Then, the computational grid is generated automatically in the computational plane (Fig. 2) by an algebraic method. The iso-I lines, which are parallel to the cascade front, are distributed with ratios 3:4:3 between the upstream:in-passage:dowstream regions. They are equidistant in the blade passage and are stretched outside it following a geometric progression law. The leading and trailing edges are positioned at mid-distance between two consecutive I stations and do not correspond to grid points so as to avoid numerical instabilities associated with the strong flow gradients encountered at the blade edges. The iso-J lines are equally spaced in the circumferential direction.

Grid Displacement

At every iteration, the grid is displaced to conform with the new position of the vibrating blades. The words old and new will be used to distinguish between two consecutive iterations. The grid points on the blades always correspond to the same physical points. The upstream and downstream boundaries remain at the same axial positions. The upstream permeable pitchwise boundaries are displaced as rigid bodies following the leading-edge displacement. The downstream permeable pitchwise boundaries are displaced following the inviscid slipstream discontinuity, which they simulate. On the displaced, as previously described, pitchwise boundaries new grid points are distributed following a geometric progression law. Care is taken that the leading and trailing edges be at mid-distance between two consecutive I stations. The new iso-I lines are straight lines joining the corresponding points on the pitchwise limits. The new iso-J lines define equidistant grid points on each iso-I line.

This grid displacement procedure preserves the nonlinear character of the formulation and permits the simulation of fairly large displacements. Furthermore, the discretization of all the interblade passages (Fig. 3) permits the simulation of an arbitrary vibratory organization of the blades, including mistuned configurations.[25,26] The method is capable of simulating arbitrary blade motion, including a profile deforming vibration mode.[2,27] However, in the applications presented here, only modes where the profile vibrates as a rigid body have been considered.

Algorithm

Numerical Scheme

The unsteady Euler equations [Eq. (1)] are written and integrated in a coordinates system fixed to the rotor. They are discretized in a moving grid by geometrically projecting the old aerodynamic field onto the new grid, following the work of Viviand and Veuillot,[28] in which the grid motion is separated from the numerical scheme. For the projection of the aerodynamic field onto the new grid, centered second-order-accurate spatial differences are used (Table 1). Then the numerical scheme is applied in the new grid (Table 1). The unsteady Euler equations are written in conservation form[29] in order to capture the shock waves eventually embedded in the flowfield following the theory of weak solutions of hyperbolic conservation laws.[30-32] The explicit predictor-corrector MacCormack scheme[33,34] is used for the integration (Table 1). It is second-order-accurate, both in time and space. Its time step is limited, for numerical stability reasons, by a CFL-type criterion.[28,35-37] In the predictor and corrector steps, forward and backward differences are used, respectively (Table 1). It is

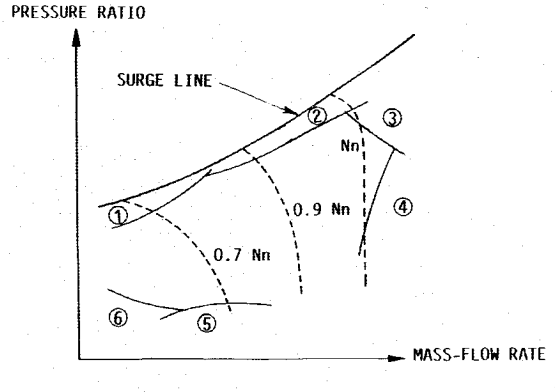

1. POSITIVE INCIDENCE SUBSONIC SEPARATION FLUTTER
2. NONSTARTED SUPERSONIC FLUTTER
3. HIGH BACK-PRESSURE STARTED SUPERSONIC FLUTTER
4. LOW BACK-PRESSURE STARTED SUPERSONIC FLUTTER
5. CHOKING FLUTTER
6. NEGATIVE INCIDENCE SUBSONIC SEPARATION FLUTTER

Fig. 1 Flutter regions on the compressor operating map.

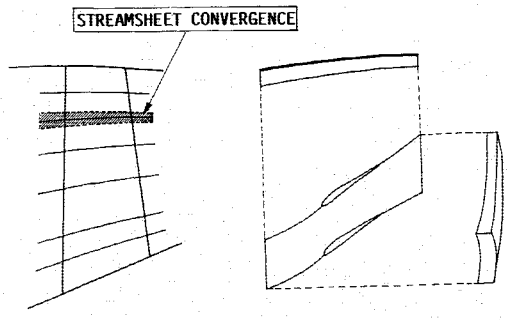

a) Blade-to-blade surface

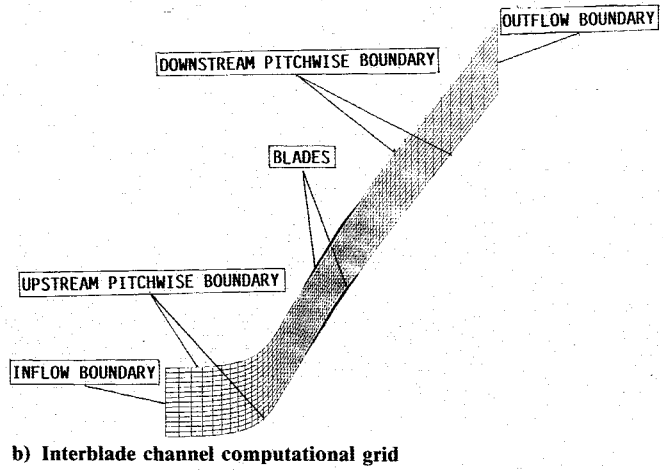

b) Interblade channel computational grid

Fig. 2 Computational domain.

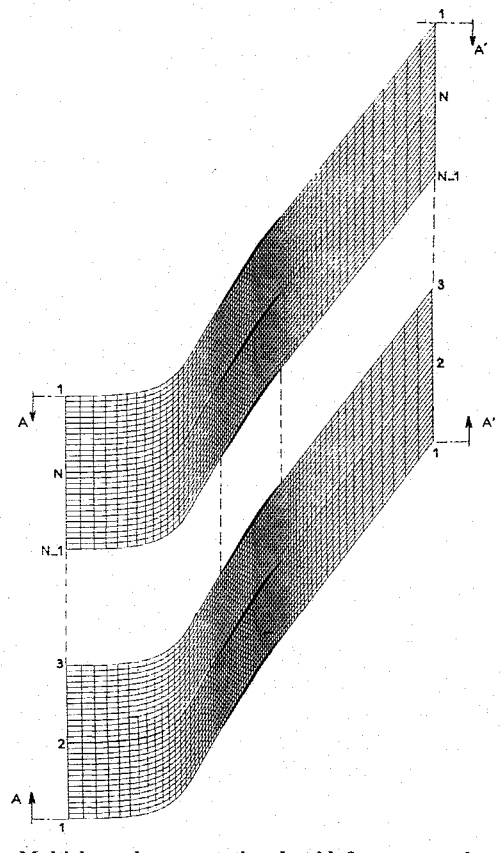

Fig. 3 Multichannel computational grid for an annular blade-to-blade surface.

Table 1 Numerical Scheme

Numerical operators

$$\Delta(.) = {}^{n+1}(.) - {}^{n}(.)$$

$${}^{\alpha\beta}\delta_i(.) = (.)_{i+\alpha} - (.)_{i-\beta}$$

$$D_i(.) = {}^{10}\delta_i(.)\ {}^{10}\delta_i(.) - {}^{01}\delta_i(.)\ {}^{01}\delta_i(.)$$

$${}^{\alpha\beta}DET = {}^{\alpha\beta}\delta_i X\ {}^{\alpha\beta}\delta_j Y - {}^{\alpha\beta}\delta_i Y\ {}^{\alpha\beta}\delta_j X$$

$${}^{\alpha\beta}\delta_X(.) = [{}^{\alpha\beta}\delta_i(.)\ {}^{\alpha\beta}\delta_j Y - {}^{\alpha\beta}\delta_i Y {}^{\alpha\beta}\delta_j(.)]/{}^{\alpha\beta}DET$$

$${}^{\alpha\beta}\delta_Y(.) = [{}^{\alpha\beta}\delta_j(.)\,{}^{\alpha\beta}\delta_i X - {}^{\alpha\beta}\delta_j X {}^{\alpha\beta}\delta_i(.)]/{}^{\alpha\beta}DET$$

$$L_i = [(\sum_{i=1,Ni} \sqrt{({}^{11}\delta_i X)^2 + ({}^{11}\delta_i Y)^2}]/(2\,Ni)$$

Numerical scheme

Grid projection	${}^{P}U = {}^{n}U + {}^{11}\delta_X {}^{n}U\,\Delta X + {}^{11}\delta_Y {}^{n}U\,\Delta Y$
Predictor step	${}^{*}U = {}^{P}U - \Delta t\,[{}^{10}\delta_X F_X({}^{P}U) + {}^{10}\delta_Y F_Y({}^{P}U) + H({}^{P}U)]$
Corrector step	${}^{**}U = \frac{1}{2}[{}^{P}U + {}^{*}U - \Delta t\,({}^{01}\delta_X F_X(U) + {}^{01}\delta_Y F_Y(U) + H(U)]$
Dissipation step	${}^{n+1}U = {}^{**}U + q\frac{\Delta t}{L_i} D_i({}^{P}U) + q\frac{\Delta t}{L_j} D_j({}^{P}U)$

necessary, in order to stabilize the numerical procedure, to use some kind of artificial dissipation. A very simple dissipative term has been adjoined to the scheme (Table 1).[38]

The discretization procedure previously described applies to internal mesh points. On the boundaries of the computational domain, inward, three-point differences are used so as to preserve second-order accuracy.[39]

Boundary Conditions

The boundary conditions are applied using the compatibility relations method.[28,40-43] The unsteady Euler equations being hyperbolic in time, they are, at every point in the flowfield, equivalent to a system of compatibility relations. On a boundary, the compatibility relations associated with ingoing characteristics are replaced by boundary conditions. Those corresponding to outgoing characteristics form, with boundary conditions, a system that is used to compute the new quantities at the boundary.[44-46] The axial velocity component is invariably subsonic in modern turbomachines.[3] Thus, at the inflow boundary, we apply three conditions by prescribing the total pressure, the total temperature, and the tangential velocity in the relative frame. A nonreflecting inflow boundary condition has also been tested.[47] For fans with no inlet distortion, the results with either of these inflow boundary conditions were practically identical. At the outflow boundary we must apply one condition, a nonreflecting condition, by prescribing the outgoing Riemann invariant.[46,47]

At the upstream permeable pitchwise boundaries, we apply a simple mathing condition between adjacent channels. On the blades, the unsteady nonpenetration condition is applied. According to the conservation of circulation theorem,[48] for every bound-vorticity change, a vortex of opposite intensity is shed in the wake of the blade. To simulate this phenomenon, we apply an inviscid slipstream condition at the downstream permeable pitchwise boundaries. This slipstream allows for tangential velocity discontinuity[49] and thus simulates the wake as a concentrated vorticity line.[14] The slip-line follows the fluid particles. Therefore, it must be displaced accordingly at every iteration.[14,31,32] The displacement velocity is determined by the normal to the slip-line component of the local fluid velocity, which is continuous.[14]

Initialization

In order to integrate in time the unsteady Euler equations, there is need for a set of initial conditions, according to the theory of hyperbolic partial-differential equations.[50] Steady-state computations are initialized by assuming that the flow is isentropic, varies linearly in space, and conforms with the boundary conditions.[46] The computed steady-state flowfield is used to initialize the unsteady flow computations.

Traveling-Wave Method

The aeromechanical eigenmodes of a tuned bladed disk, i.e., of a bladed disk of perfect cyclic symmetry, are traveling waves.[51-52] All of the blades vibrate at the same mode and frequency but are out of phase, one with respect to its neighbors, by a phase angle that is constant along the circumference.[51] For every blade mode there are N different traveling waves,

$$q_k = q \sin[\omega t + (k-1)\beta_r], \quad \left(\beta_r = \frac{2\pi}{N} r;\ r = 0,\ldots,N-1\right), \quad (k = 1,\ldots,N) \tag{5}$$

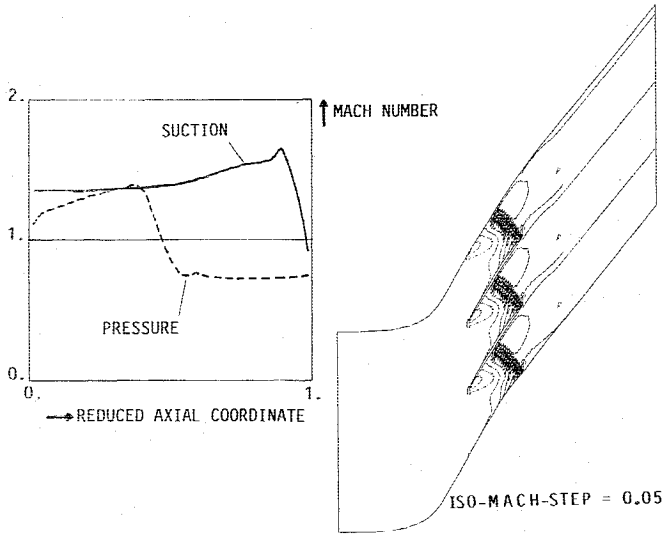

Fig. 4 Steady-state Mach number distribution for fan A started-flow configuration.

Table 2 Features of the fan blades studied

	Fan A	Fan B
Nominal rotation rate, rpm	9551	10,600
Span, %	92	96
Radius, mm	376.3	396.3
Chord, mm	154.7	133.3
Solidity	1.44	1.23
Number of blades	22	23
Stagger angle, deg	33.8	27.6

Thus, there exists a periodicity that relates the phase of vibration to the angular position of the blade. It is usual, in the case of traveling-wave modes, to perform the computation in a single channel by applying this chorochronical periodicity condition at the permeable pitchwise boundaries.[10,12,14,15] This permits a considerable gain in computational time.

In the present work, a traveling-wave method has been developed. In order to apply the described chorochronical periodicity, one needs to know the vibration in time of the scheme variables at the permeable pitchwise boundaries. To this end, their values are stored in computer memory for a number of instants per period (usually 72). Then their value at a given instant is computed using a piecewise quintic interpolation procedure inspired by the interpolation method proposed by Akima.[53] Fourth-order-accurate Taylor expan-

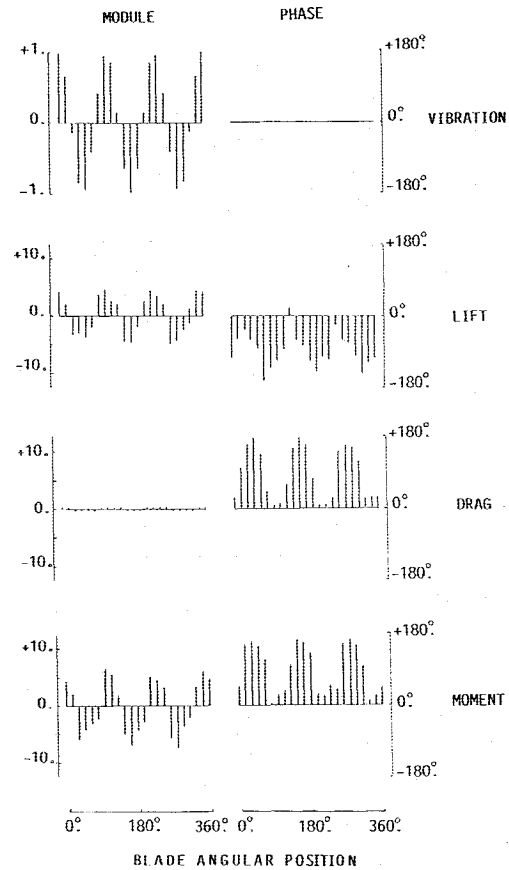

Fig. 5 Modules and phases of the generalized aerodynamic forces first harmonic for fan A standing-wave vibration.

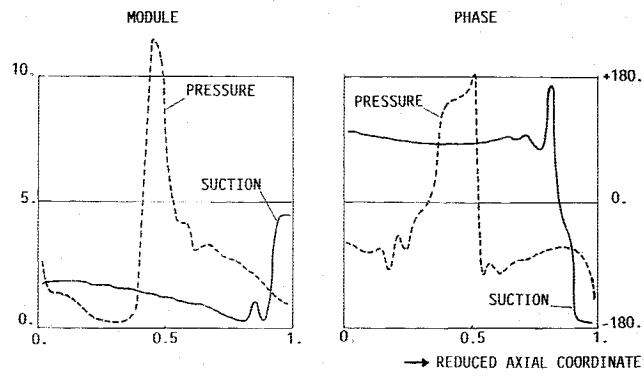

Fig. 6 Pressure coefficient first harmonic distribution on blade 1 for fan A standing-wave vibration.

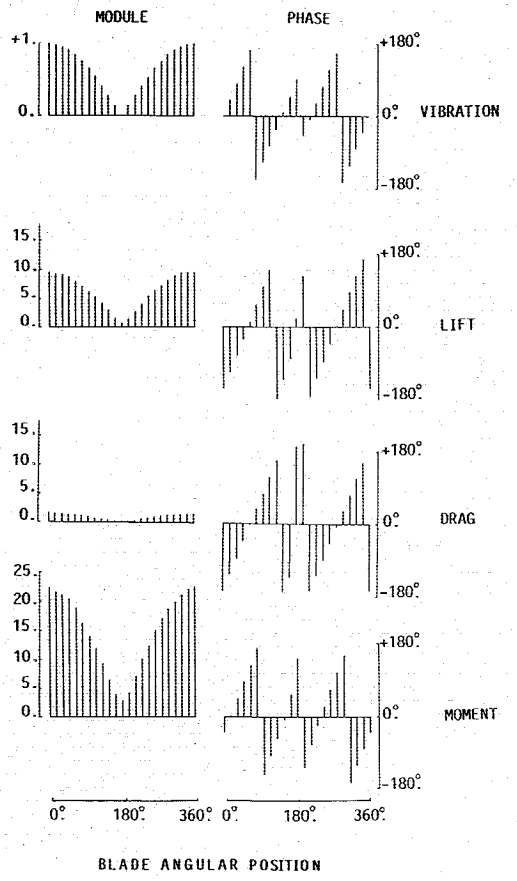

Fig. 7 Modules and phases of the generalized aerodynamic forces first harmonic for fan A mistuned vibration.

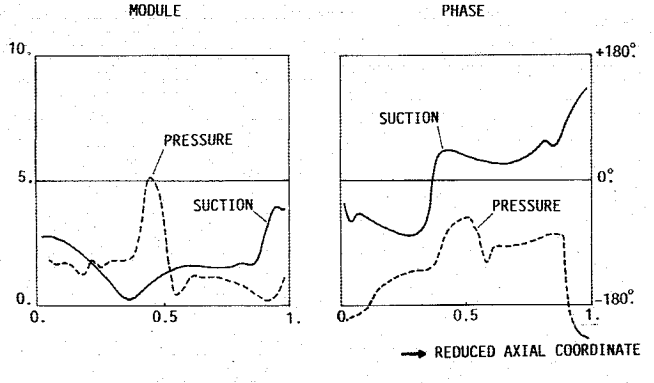

Fig. 8 Pressure coefficient first harmonic distribution on blade 1 for fan A mistuned vibration.

sions[54] are used to evaluate slopes and curvatures. No special attention is due to end-of-period points, since all functions are cyclic in time.

Influence-Wave Method

It is usual, both in experimental work[55,56] and theoretical formulations,[52] to study configurations where only one blade vibrates, all the others being constrained to inertia, which we shall call influence waves. The multichannel method may readily simulate such configurations. However, experimental results[55,56] and experience with the multichannel method indicate that the influence of the vibrating blade attenuates rapidly as one moves away from it along the circumference. Thus, one may gain in computational time by truncating the cascade to a limited number of channels (seven channels were retained). The center blade vibrates and steady-state distributions are prescribed throughout the computation at the truncation boundaries. This is equivalent to assuming that the unsteady effects are negligible after the truncation.

Results

Cases Studied

To demonstrate the methodology's possibilities, we will present results for two fan blades, whose main characteristics are summarized in Table 2. Standing-wave vibration and mistuned vibration results, computed with the multichannel method (*MC*), are presented for a started flow condition of fan A. Traveling-wave vibration results, computed with the traveling-wave method (*TW*), the multichannel method (*MC*), and the influence-wave method (*IW*), are presented for an unstarted flow condition of fan B. A 80 × 15 (axial × pitchwise/channel) grid was used in all the computations.

Fan A – Started Flow – Standing Wave

A standing-wave vibration at the nominal operating point of fan A (Table 2) will be examined first. The relative upstream Mach number is 1.32, and the flow is started with a strong in-passage shock wave (Fig. 4). The blade vibration is in bending perpendicular to the chord, and the assembly mode is a 3ϕ standing wave (Fig. 5). The vibration frequency is 900 Hz ($Sr_\chi = 0.33$). All the blades vibrate in phase, and the maximum blade amplitude is 1 mm. The computation was performed in all of the 22 interblade channels. The first harmonic of the generalized aerodynamic forces is presented in Fig. 5. The moment amplitude is in percent of the steady-state value, and the spanwise and edgewise forces are in percent of the total steady-state force. The moment is computed around the torsional center, which is situated near midchord. The standing-wave pattern of the flow response is evident. The first harmonic pressure coefficient on blade 1 is presented in Fig. 6. The amplitude peaks at the locations of the shock waves may be noticed.

Fan A – Started Flow – Mistuned Vibration

Results will be presented for a mistuned vibration pattern, at the nominal operating point of fan A (Fig. 4). The blade vibration mode is torsional around the section's torsional center, which is situated near midchord. The vibration frequency is 1000 Hz ($Sr_\chi = 0.30$). The assembly mode is the superposition of two traveling waves of amplitude 0.5 deg and of orders + 2 and + 3, respectively (Fig. 7). The computation was performed in all of the 22 interblade chanels. The first harmonic of the pressure coefficient on blade 1 is depicted in Fig. 8.

Fan B – Unstarted Flow – Traveling Wave

In order to demonstrate the method's potential in the region of unstarted flow, results are presented for an operating point of 87% of design speed of fan B. The relative upstream Mach number is 1.25, and the flow is nonstarted due to the relatively high back-pressure level, with a system of detached strong shock waves (Fig. 9). The incidence is 2.5 deg above the unique incidence angle.[17,18] The blades vibrate in torsion around midchord at a frequency of 780 Hz ($Sr_\chi = 0.25$), and the amplitude is 1 deg. The assembly mode is a second-order traveling wave ($\beta_r = -31.30$ deg). Both the traveling-wave method and the multichannel method have been used to compute this configuration. The distribution of the first harmonic of the pressure coefficient on the blade is presented in Fig. 10. The amplitude peaks at the shock-wave foot, on the pressure-side and at the leading edge, may be noticed. The amplitude peaks at the leading edge are due to the detached shock-wave system. The comparison between the traveling-wave method and the multichannel method shows very good agreement. The traveling-wave method is, however, about 23 times faster (Table 3), since this rotor has 23 blades, and the multichannel method simulates all the interblade channels. The interest of the multichannel method is in its capability of simulating arbitrary assembly modes of vibration.

Table 3 Computational time requirements

Case	Method	Channels	Frequency, Hz	Sr_x	CPU/channel/ period, min	CPU/ period, min	CPU (six periods), min
Standing wave	*MC*	22	900	0.33	1.7	38.3	229.8
Mistuned mode	*MC*	22	1000	0.36	1.5	32.7	196.2
Traveling wave	*TW*	1	780	0.25	2.3	2.3	13.8
	MC	23	780	0.25	2.1	48.3	289.7
	IW	7	780	0.25	2.1	28.6	88.7
Started flow comparison	*IW*	7	356	0.12	4.1	28.6	171.6
Nonstarted flow comparison	*IW*	7	136	0.06	7.1	49.7	298.2

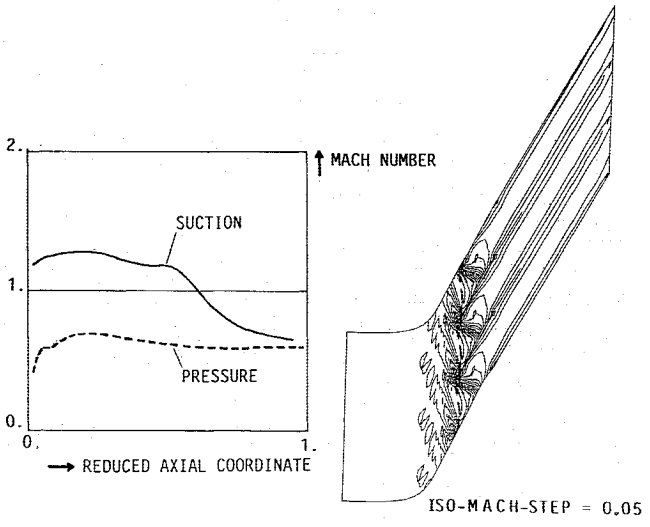

Fig. 9 Steady Mach number distribution for fan B unstarted-flow configuration.

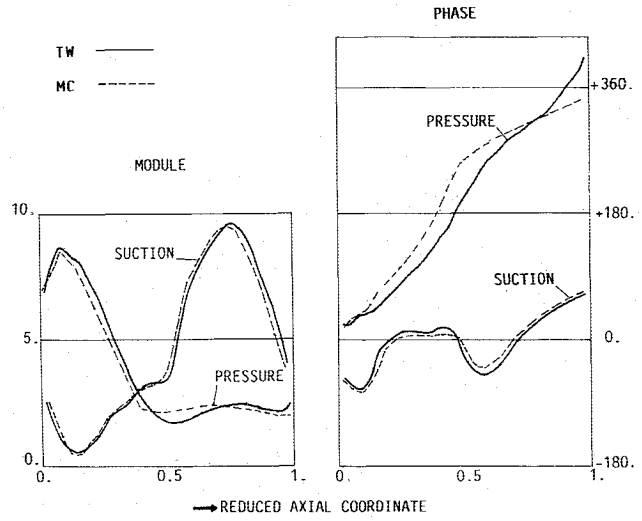

Fig. 10 Pressure coefficient first harmonic distribution for fan B traveling-wave vibration and comparison between the standing-wave method and the multichannel method.

The reason for truncating the cascade to a limited number of channels in the influence-wave method is computational time economy. The least number of channels giving satisfactory results must be retained. In Fig. 11, the imaginary part of the first harmonic of the aerodynamic moment is presented as a function of interblade phase angle. The moment is in percent of its steady-state value. Symbols denote values predicted directly by a traveling-wave method, which may be considered as the most reliable result. Lines denote results obtained by superposition of the influence coefficients, computed using the influence-wave method using different numbers of channels in the truncated cascade. Results with five channels are not quite satisfactory. Results using seven channels predict correctly the main features of the traveling-wave results, while using nine channels in the computation does not offer any substantial improvement in the prediction. From a number of similar results not presented here, this author believes that, for solidities like those of fans A and B, seven channels is a judicious choice.

Comparison with Experimental Data

Cases Studied

The value of a methodology resides in its potential to simulate realistic flow configurations. A first validation of the methods is attempted here, through comparison with available experimental data from detailed measurements performed by ONERA.[57] The experimental setting[56,58] consists of a rectilinear cascade of nine blades, where the center blade vibrates, all the others being constrained to inertia. The measurement of the influence coefficients permits the reconstruction of the unsteady aerodynamic forces for an arbitrary vibratory

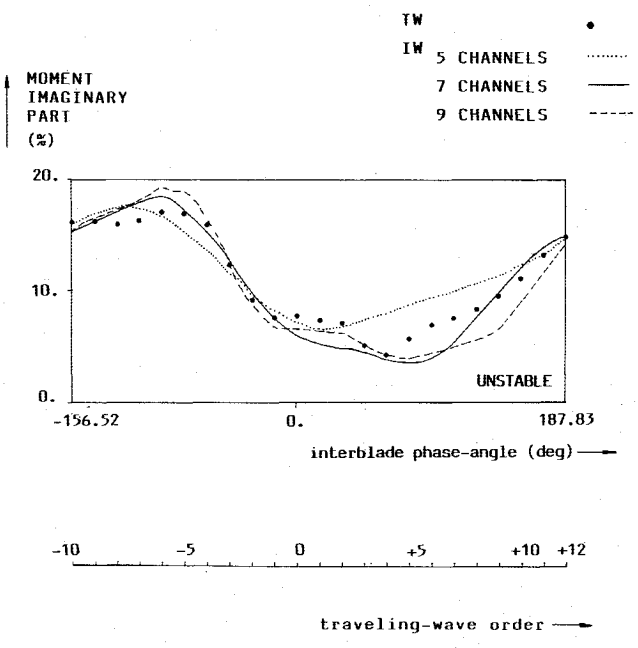

Fig. 11 Imaginary part of the first harmonic of the aerodynamic moment vs interblade phase angle for fan B traveling-wave vibration and comparison between the standing-wave method and the multichannel method.

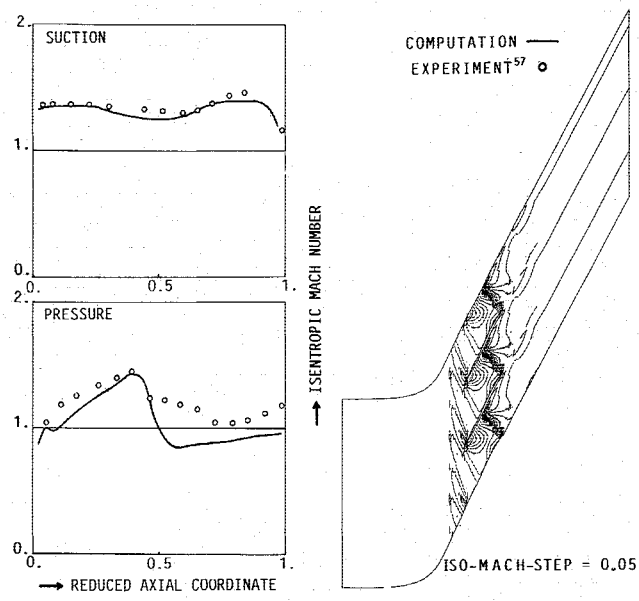

Fig. 12 Comparison of computed and measured isentropic Mach number distribution for fan B started-flow configuration.

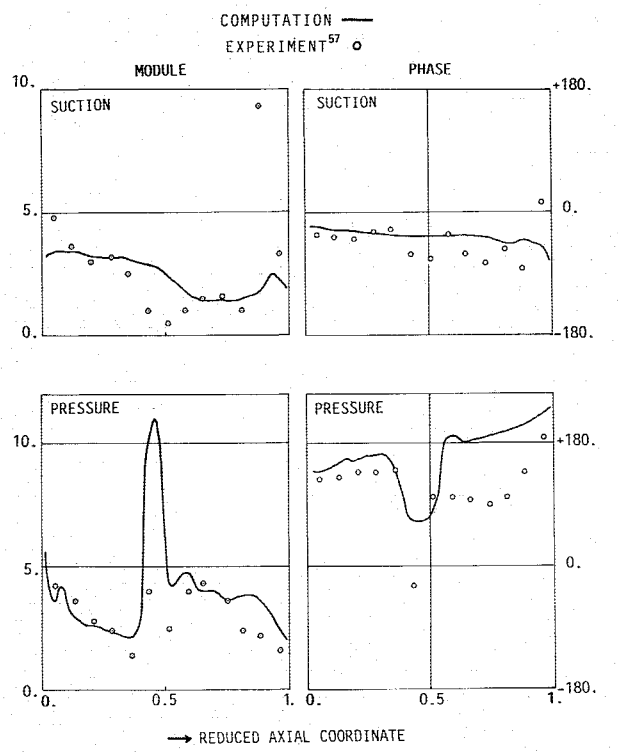

Fig. 13 Comparison of computed and measured pressure coefficient first harmonic distribution on the vibrating blade for fan B influence-wave vibration.

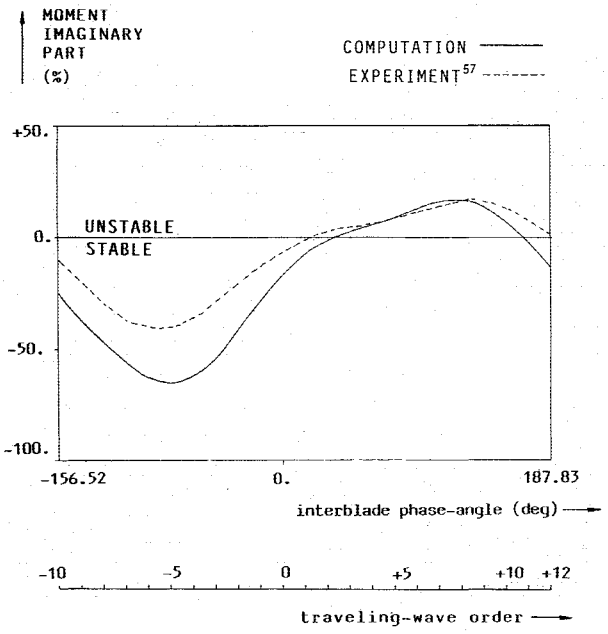

Fig. 14 Comparison of the curves for the first harmonic of the aerodynamic moment vs interblade phase angle for fan B vibration, reconstructed using computed and measured influence coefficients, respectively.

mode.[52] Comparisons are presented below of computed and measured unsteady pressure distributions for a started flow configuration of fan B and for an unstarted flow configuration of fan A. The influence-wave method was used to compute the unsteady flow response.

Fan B – Started Flow

The steady-state flow is started (Fig. 12) with a strong in-passage shock wave. The upstream Mach number is on the order of 1.4, and the back-pressure is relatively low. One may notice the strong (supersonic-to-subsonic) leading-edge shock wave on the pressure side and the subsequent acceleration until the strong in-passage shock wave. The comparison between computed and measured[57] isentropic Mach number distributions shows satisfactory agreement, with the exception of the shock-wave/boundary-layer interaction region on the pressure side, where viscous effects become important. This overprediction of postshock pressure recovery is typical of inviscid methods.[18,59]

The unsteady results are for a purely torsional mode, around midchord at a frequency of 356 Hz ($Sr_x = 0.12$). The comparison (Fig. 13) of the computed and measured[57] pressure coefficient first harmonic on the vibrating blade shows rather satisfactory agreement, with the exception of the phase angle in the shock-wave/boundary-layer interaction region on the pressure side. It would seem that only a method adequately accounting for the viscous effects might accurately simulate the flow in this region.

In order to make a flutter estimate, one needs to know the generalized unsteady aerodynamic forces on the blades. Figure 14 depicts the imaginary part of the first harmonic of the aerodynamic moment, in percent of its steady-state value, as a function of interblade phase angle. The results obtained by superposition of the computed influence coefficients are compared to those obtained by superposition of the measured influence coefficients. The comparison is quite satisfactory, especially in the region of unstable interblade phase angles.

Fan A – Unstarted Flow

The steady-state flow is unstarted (Fig. 15). The upstream Mach number is on the order of 1.2. The comparison of computed and measured[57] isentropic Mach number distributions shows satisfactory agreement (Fig. 15 shows the accurate prediction of the shock-wave location on the suction side). However, the postshock pressure recovery is again overpredicted,[18,58] and on the pressure side there is a noticeable difference in Mach number level. These discrepancies were attributed to viscous effects. Also, a weak leading-edge shock wave was not resolved by the method. It is not clear whether this discrepancy must be attributed to viscous phenomena or to insufficient algorithm resolution of the leading-edge detached shock structure.

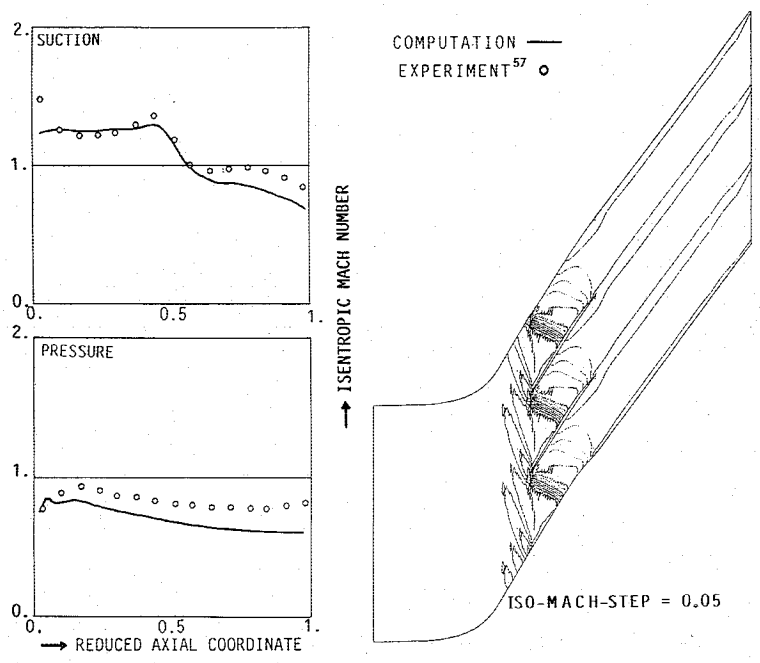

Fig. 15 Comparison of computed and measured isentropic Mach number distribution for fan A unstarted-flow configuration.

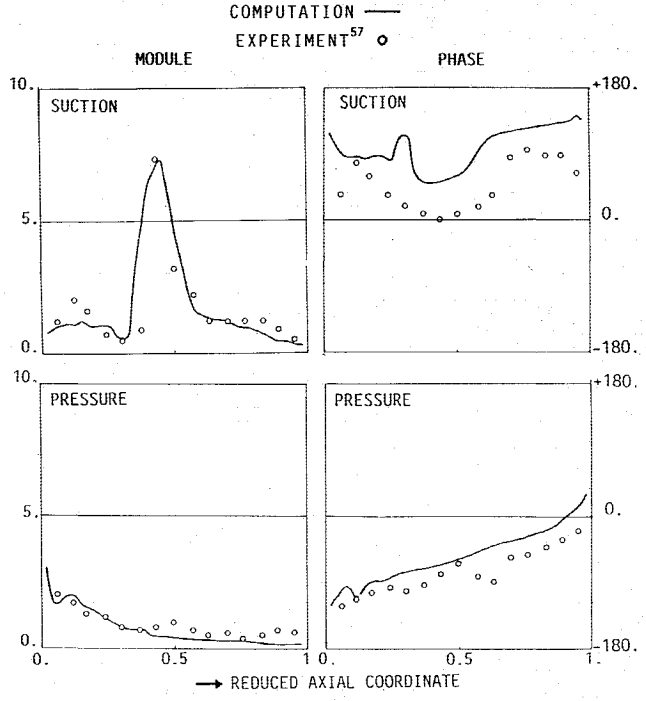

Fig. 16 Comparison of computed and measured pressure coefficient first harmonic distribution on the vibrating blade for fan A influence-wave vibration.

The unsteady results are for a pure bending mode perpendicular to the chord. The frequency is 136 Hz ($Sr_{\dot{x}} = 0.06$). The comparison of computed and measured[57] pressure coefficient first harmonic distributions on the vibrating blade shows very good agreement (Fig. 16), with the exception of the phase angle on the suction side, due mainly to the insufficient leading-edge shock system resolution and the viscous effects in the shock-wave/boundary-layer interaction on the suction side.

Computational Time Requirements

All the computations were performed on an IBM 3090-200 computer. Convergence of the unsteady results (harmonics) was satisfactory after simulating six vibration periods. Computational time requirements for the results presented here may be found in Table 3.

Conclusions

In the present work, a Euler solver has been developed for analyzing the blade-to-blade surface unsteady aerodynamics of vibrating cascades. The method may simulate cascades of arbitrary geomentry and is completely nonlinear with vibration amplitude. Both started and unstarted flow configurations may be simulated, as may be seen from the results presented. The method provides both the steady-state flowfield and its response to the vibration of the blades.

The multichannel method has the capability of directly simulating complex and arbitrary assembly modes, such as standing waves, influence waves, and mistuned modes. A much faster traveling-wave method has also been developed to simulate the flow in a single channel to analyze the flowfield response to traveling waves. Finally, a truncated multichannel influence-wave method has also been developed.

Throughout this work we were aware that viscous effects must be included in the modeling. However, a first comparison with experimental results demonstated the ability of the method to reproduce quantitatively the unsteady flow in vibrating cascades with supersonic started or unstarted flows. Although viscous effects produce discrepancies between computation and experiment, the results are globally quite satisfactory.

We believe that this methodology provides a powerful analytic tool for the unsteady aerodynamics of vibrating cascades in the supersonic flow regime. It may simulate with accuracy realistic configurations in actual aircraft engine fans. The modeling of viscous effects will not only enhance the method's accuracy but also extend its applicability to the subsonic flutter regions, thus permitting flutter analysis everywhere in the compressor operating map.

Acknowledgments

This research was conducted at the Aerodynamics Department of SNECMA. The author is very grateful to the direction of SNECMA for its permission to publish this paper.

References

[1]Lubomski, J. F., "Status of NASA Full-Scale Engine Aeroelasticity Research," AIAA Paper 80-36906, 1980.

[2]Mikolajczak, A. A., Arnoldi, R. A., Snyder, L. E., and

Stargardter, H., "Advances in Fan and Compressor Blade Flutter Analysis and Predictions," *Journal of Aircraft*, Vol. 12, April 1975, pp. 325–332.

[3]Carta, F. O., "Aeroelasticity and Unsteady Aerodynamics," *Aerothermodynamics of Aircraft Gas Turbine Engines*, edited by G. C. Oates, AFAPL-TR-78-52, 1978, Chap. 22.

[4]Sisto, F., "A Review of the Fluid Mechanics of Aeroelasticity in Turbomachines," *ASME Journal of Fluids Engineering*, Vol. 99, March 1977, pp. 40–44.

[5]Platzer, M. F., "Transonic Blade Flutter – A Survey," *Shock and Vibration Digest*, Vol. 7, July 1975, pp. 97–106.

[6]McNally W. D. and Sockol, P. M., "Computational Methods for Internal Flows with Emphasis on Turbomachinery," NASA TM-82764, 1981.

[7]Chapman, D. R., "Computational Aerodynamics Development and Outlook," *AIAA Journal*, Vol. 17, Dec. 1979, pp. 1293–1313.

[8]"Report of the Working Group on Large-Scale Computing in Aeronautics," AGARD AR-209, 1984.

[9]Kutler, P., "A Perspective of Theoretical and Applied Computational Fluid Dynamics," *AIAA Journal*, Vol. 23, March 1985, pp. 328–341.

[10]Whithead, D. S., "The Calculation of Steady and Unsteady Transonic Flow in Cascades," CUED/A-Turbo/TR -/18, 1982.

[11]Namba, M. and Ishikawa, A., "3D Aerodynamic Characteristics of Oscillating Supersonic and Transonic Annular Cascades," *ASME Journal of Engineering for Power*, Vol. 105, Jan. 1983, pp. 138–146.

[12]Verdon J. H. and Caspar, J. R., "A Linearized Unsteady Aerodynamic Analysis for Transonic Cascades," *Journal of Fluid Mechanics*, Vol. 149, 1984, pp. 403–429.

[13]Mortchelewicz, G. D. and Angelini, J. J., "Computation of Unsteady Aerodynamic Pressure Coefficients in a Transonic Straight Cascade," *Unsteady Aerodynamics of Turbomachines and Propellers*, International Union of Theoretical and Applied Mechanics, Cambridge, England, 1984.

[14]Pandolfi, M., "Numerical Experiments on Unsteady Flow through Vibrating Cascades," *Aeroelasticity of Turbomachines*, International Union of Theoretical and Applied Mechanics, Lausane, Switzerland, 1980.

[15]Joubert, H., "Supersonic Flutter in Axial Flow Compressors," *Unsteady Aerodynamics of Turbomachines and Propellers*, International Union of Theoretical and Applied Mechanics, Cambridge, England, UK, 1984.

[16]Starken, H. and Lichtfuss,, H. J., "Supersonic Cascade Performance," AGARD LS-39, 1970.

[17]Leynaert, J., "Modes de Fonctionnement des Grilles d'Aubes" ONERA, France, NT-1/7122-AN, 1973.

[18]Tijdeman, H. and Seebas, R., "Transonic Flow past Oscillating Airfoils," *Annual Review of Fluid Mechanics*, Vol. 12, 1980, pp. 181–222.

[19]Davies, M. R. D. and Bryanston-Cross, P. J. "Holographic Measurements and Theoretical Predictions of the Unsteady Flow in a Transonic Annular Cascade," *American Society of Mechanical Engineers*, New York, ASME Paper 84-GT-174, 1984.

[20]Williams, M. H., "Linearization of Unsteady Transonic Flow Containing Shocks," *AIAA Journal*, Vol. 17, April, 1979, pp. 394–397.

[21]Williams, M. H., "Unsteady Thin Airfoil Theory for Transonic Flow with Embedded Shocks," *AIAA Journal*, Vol. 18, June 1980, pp. 615–624.

[22]Wu, C.-H., "A General Theory of 3D Flow in Subsonic and Supersonic Turbomachines of Axial-, Radial-, and Mixed-Flow Types," *ASME Transactions*, Vol. 74, Nov. 1952, pp. 1363–1380.

[23]Crocco, L., "A Suggestion for the Numerical Solution of the Steady Navier-Stokes Equations," *AIAA Journal*, Vol. 3, Oct. 1965, pp. 1824–1832.

[24]Chima, R. V., "Development of an Exhibit Multigrid Algorithm for Quasi-3D Viscous Flows in Turbomachinery, AIAA Paper 86-0032, 1986.

[25]Whithead, D. S., "Torsional Flutter of Unstalled Cascade Blades at Zero Deflection," Aeronautical Research Council, ARC R&M 3429, 1965.

[26]Ewins, D. J., "The Effects of Detuning Upon the Forced Vibrations of Bladed Disk," *Journal of Sound and Vibration*, Vol. 9, pp. 65–79.

[27]Arnoldi, R. A., Carta, F. O., St. Hilaire, A. O., and Dalton, W. N., III, "Chordwise Bending Flutter in Cascades," Pratt and Whitney Aircraft, Rept. PWA 5271, 1975.

[28]Viviand, H. and Veuillot, J. P., "Méthodes Pseudo-Instationnaires pour le Calcul d'Écoulements Transsoniques," ONERA, France, TP-1978-4, 1978.

[29]Viviand, H., "Formes Conservatives, des Équations de la Dynamique des Gaz," *La Recherche Aérospatiale*, Vol. 1974-1, Jan./Feb. 1974, pp. 65–68.

[30]Lax, P. D., "Weak Solutions of Nonlinear Hyperbolic Equations and their Computation," *Communications on Pure and Applied Mathematics*, Vol. 8, 1954, pp. 159–193.

[31]Lax, P. D., "Hyperbolic Systems of Conservation Laws," *Communications on Pure and Applied Mathematics*, Vol. 10, 1957, pp. 537–566.

[32]Lax, P. D. and Wendroff, B., "Systems of Conservation Laws," *Communications on Pure and Applied Mathematics*, Vol. 13, 1960, pp. 217–237.

[33]MacCormack, R. W., "The Effect of Viscosity on Hypervelocity Impact Cratering," AIAA Paper 69-354, 1969.

[34]MacCormack, R. W., "Numerical Solution of the Interactions of a Shock Wave with a Laminar Boundary Layer," *Numerical Methods in Fluid Dynamics*, *Lecture Notes in Physics*, Vol. 8, 1971, pp. 151–163.

[35]Courant, R., Friedrichs, K. O., and Lewy, H., "On the Partial Difference Equations of Mathematical Physics," *IBM Journal*, March 1967, pp. 215–234.

[36]Veuillot, J. P., "Calcul Numérique de l'Écoulement Transsonique d'un Fluide Parfait dans une Grille d'Aubes," *La Recherche Aérospatiale*, Vol. 1975-6, Nov.–Dec. 1975, pp. 327–338.

[37]Veuillot, J. P., "Calculation of the Quasi-3D Flow in a Turbomachine Blade Row," *ASME Journal of Engineering for Power*, Vol. 99, Jan. 1977, pp. 53–62.

[38]Lerate, A. and Sides, J., "Calcul Numerique d'Écoulements Transsoniques Instationnaires," ONERA, France, TP-1977-19F, 1977.

[39]Kutler, P., Reinhardt, W. A., and Warming, R. F., "Multishocked 3D Supersonic Flowfields with Real Gas Effects," *AIAA Journal*, Vol. 11, May 1973, pp. 657–664.

[40]Moretti, G., "Importance of Boundary Conditions in the Numerical Treatment of Hyperbolic Equations," *The Physics of Fluids*, Supplement II, 1969, pp. 13–20.

[41]Gopalakrishnan, S. and Bozzola, R., "Numerical Representation of Inlet and Exit Boundary Conditions in Transient Cascade Flow," American Society of Mechanical Engineers, ASME New York, Paper 73-GT-55, 1973.

[42]Porter, R. W. and Coakley, J. F., "Use of Characteristics for Boundaries in Time Dependent Finite-Difference Analysis of Multi-Dimensional Gas-Dynamics," *International Journal for Numerical Methods in Engineering*, Vol. 5, 1972, pp. 91–101.

[43]Brochet, J., "Calcul Numérique d'Écoulements Internes 3D Transsoniques," *La Recherche Aérospatiale*, Vol. 1980-5, Sept.–Oct. 1980, pp. 301–315.

[44]Cambier, L., Ghazzi, W., Veuillot, J. P., and Viviand, H., "Une Approche par Domaines pour le Calcul d'Écoulements Compressibles," ONERA, TP-1981-143, 1981.

[45]Sovrano, R., "Calcul de l'Écoulement Transsonique dans un Compresseur Centrifuge par une Méthode Psuedo-Instationnaire," ONERA, France, TP-1980-42, 1980.

[46]Veuillot, J. P. and Meauzé, G., "A 3D Euler Method for Internal Transonic Flow Computation with a Multi-Domain Approach," AGARD LS 140, Paper 5, 1985.

[47]Hedstrom, G. W., "Nonreflecting Boundary Conditions for Nonlinear Hyperbolic Systems," *Journal of Computational Physics*, Vol. 30, 1979, pp. 222–237.

[48]Mobbs, S. D., "Some Vorticity Theorems and Conservation Laws for Nonbarotropic Fluids," *Journal of Fluid Mechanics*, Vol. 108, 1981, pp. 475–483.

[49]Liepmann, H. and Roshko, A., *Elements of Gasdynamics*, Wiley, New York, 1957, pp. 101–109.

[50]Courant, H. and Hilbert, D., "Methods of Mathematical Physics," Wiley Interscience, New York, 1962, pp. 39–56.

[51]Lane, F., "System Mode Shapes in the Flutter of Compressor Blade Rows," *Journal of the Aeronautical Sciences*, Vol. 23, Jan. 1956, pp. 54–66.

[52]Crawley, E. F., "Aeroelastic Formulations for Turbomachines and Propellers," *Unsteady Aerodynamics of Turbomachines and Propellers*, International Union of Theoretional and Applied Mechanics, 1984.

[53]Akima, H., "A New Method of Interpolation and Smooth Curve Fitting Based on Local Procedures," *Journal of the Association for Computing Machinery*, Vol. 17, Oct. 1970, pp. 589–602.

[54]Roache, P. J., *Computational Fluid Dynamics*, Hermosa Publishing, Albuquerque, NM, 1976, pp. 18–21.

[55]Hanamura, Y., Tanaka, H., and Yamaguchi, K., "A Simplified Method to Measure Unsteady Forces Acting on the Vibrating Blades

in Cascade," *Bulletin of the Japanese Society of Mechanical Engineers*, Vol. 23, June 1980, pp. 880–887.

[56]Girault, J. P., "Le Flottement de Flexion en Régime Supersonique Amorcé," *La Recherche Aérospatiale*, Vol. 1984-1, Jan.–Feb. 1984, pp. 57–66.

[57]Cafarelli, I., private communication, ONERA, Châtillon, France, 1986.

[58]Széchényi, E. and Finas, R., "Aeroelastic Testing in a Straight Cascade Wind Tunnel," *Aeroelasticity in Turbomachines*, International Union of Theoretical and Applied Mechanics, Lausane, Switzerland, 1980.

[59]Tijdeman, H., "Investigation of the Transonic Flow Around Oscillating Airfoils," Ph.D. Thesis, Delft Technological University, Delft, the Netherlands, 1977.